

This discussion paper is/has been under review for the journal Atmospheric Chemistry and Physics (ACP). Please refer to the corresponding final paper in ACP if available.

# Top-down estimates of biomass burning emissions of black carbon in the Western United States

Y. H. Mao<sup>1</sup>, Q. B. Li<sup>1,2</sup>, J. T. Randerson<sup>3</sup>, D. Chen<sup>1,2,\*</sup>, L. Zhang<sup>1,2,\*\*</sup>, W. M. Hao<sup>4</sup>, and K.-N. Liou<sup>1,2</sup>

<sup>1</sup>Department of Atmospheric and Oceanic Sciences, University of California, Los Angeles, CA 90095, USA

<sup>2</sup>Joint Institute for Regional Earth System Science and Engineering, University of California, Los Angeles, CA 90095, USA

<sup>3</sup>Department of Earth System Science, University of California, Irvine, CA 92697, USA

<sup>4</sup>Fire Sciences Laboratory, U.S. Forest Service, Missoula, MT, 59808, USA

\* now at: National Center for Atmospheric Research, Boulder, CO 80307, USA

\*\* now at: Department of Mechanical Engineering, University of Colorado Boulder, Boulder, CO 80302, USA

Received: 27 February 2013 – Accepted: 15 April 2013 – Published: 30 October 2013

Correspondence to: Q. B. Li (qli@atmos.ucla.edu)

Published by Copernicus Publications on behalf of the European Geosciences Union.

Top-down estimates  
of biomass burning  
emissions of black  
carbon

Y. H. Mao et al.

Title Page

Abstract

Introduction

Conclusions

References

Tables

Figures

⏪

⏩

◀

▶

Back

Close

Full Screen / Esc

Printer-friendly Version

Interactive Discussion

## Abstract

We estimate biomass burning emissions of black carbon (BC) in the western United States (WUS) for May–October 2006 by inverting surface BC concentrations from the Interagency Monitoring of PROtected Visual Environment (IMPROVE) network using a global chemical transport model. We first improve the spatiotemporal distributions of the BC emissions from the Global Fire Emissions Database (GFEDv2) using 8-day active fire counts from the Moderate Resolution Imaging Spectroradiometer (MODIS) from a 3 yr period (2005–2007). The resulting emissions are then used as the a priori for the inversion analyses. The adjustment primarily shifts emissions from late to early and middle summer (33 % decrease in September–October and 56 % increase in June–August). The adjusted emissions lead to non-negligible increases in the simulated surface BC concentrations in early and middle summer at sites below 2 km. We conduct analytical inversions at both  $2^\circ \times 2.5^\circ$  and  $0.5^\circ \times 0.667^\circ$  (nested over North America) horizontal resolutions. Simulated surface BC concentrations with the a posteriori emissions capture the observed major fire episodes at many sites and substantial enhancements at the 1–2 and 2–3 km altitude ranges. The a posteriori emissions lead to substantial bias reductions in the simulated surface BC concentrations ( $\sim 50\%$  on average) at both resolutions and significant increases in the Taylor skill scores (86 % at  $2^\circ \times 2.5^\circ$  and 132 % at  $0.5^\circ \times 0.667^\circ$ ). We find that the inversion is rather sensitive to the model resolution. The a posteriori biomass burning emissions increase by factors of 4.7 from the inversion at  $2^\circ \times 2.5^\circ$  and 2.8 at  $0.5^\circ \times 0.667^\circ$ , while as the a posteriori anthropogenic emissions decrease by 48 % and 36 %, respectively, relative to their corresponding a priori emissions. The two a posteriori estimates differ largest in biomass burning emissions in California and the Southwest (a factor of 5.9) and in the Pacific Northwest (a factor of 2).

28068

ACPD

13, 28067–28115, 2013

## Top-down estimates of biomass burning emissions of black carbon

Y. H. Mao et al.

Title Page

Abstract

Introduction

Conclusions

References

Tables

Figures

⏪

⏩

◀

▶

Back

Close

Full Screen / Esc

Printer-friendly Version

Interactive Discussion





## Top-down estimates of biomass burning emissions of black carbon

Y. H. Mao et al.

Title Page

Abstract

Introduction

Conclusions

References

Tables

Figures

⏪

⏩

◀

▶

Back

Close

Full Screen / Esc

Printer-friendly Version

Interactive Discussion

main in the temporal variations and spatial distributions of fire emissions, particularly from burned area and fuel load (Langmann et al., 2009). Small fires are likely a major source of uncertainty in the estimates of biomass burning emissions of BC (Randerson et al., 2012). For instance, small fires can lead to high relative errors of 50–100 % in the burned area estimates (Giglio et al., 2006, 2010). Additionally, the lack of detection of agricultural burnings may be another large uncertainty (Randerson et al., 2012; van der Werf et al., 2010; McCarty et al., 2009; Roy and Boschetti, 2009; Korontzi et al., 2006).

Understanding the distribution of a chemical species in the atmosphere depends on the information of the emissions. The bottom-up emission estimates generally rely on emission factors using socioeconomic, energy, land use or environmental data (Heald et al., 2004). In recent years, there has been an increasing emphasis on the use of inverse methods to characterize the temporal and spatial variability of emissions. Inverse modeling is a standard tool for estimating top-down emissions from the combination of observations of atmospheric trace species and bottom-up constraints using a forward model  $F(\mathbf{x})$ . Considering the general problem of estimating a set of emissions (assembled in a state vector  $\mathbf{x}$ ), given a set of observed atmospheric concentrations (observation vector  $\mathbf{y}$ ) with error  $\boldsymbol{\varepsilon}$ , we relate  $\mathbf{x}$  to  $\mathbf{y}$  by the following relation (Rodgers, 2000):

$$\mathbf{y} = F(\mathbf{x}) + \boldsymbol{\varepsilon} \quad (1)$$

Based on Bayes' theorem and the assumption of Gaussian error distributions (Rodgers, 2000), the optimal or Maximum A Posteriori (MAP) solution for  $\mathbf{x}$  by given  $\mathbf{y}$ , is equivalent to find the minimum in an error-weighted least squares scalar cost function  $J(\mathbf{x})$  (that is, to solve  $\nabla_{\mathbf{x}}J(\mathbf{x}) = 0$ ). The cost function describes the error-weighted mismatch between the observed concentrations,  $\mathbf{y}$ , and those simulated with the forward model,  $F(\mathbf{x})$ , as well as the error-weighted mismatch between the true state and the a priori estimate  $\mathbf{x}_a$  (Kopacz et al., 2009). Most of the inverse modeling literature for atmospheric composition has used an analytical solution for  $\nabla_{\mathbf{x}}J(\mathbf{x}) = 0$ . Applications of analytical in-







its moisture content (Langmann et al., 2009). For GFED, the Carnegie-Ames-Stanford-  
Approach (CASA) biogeochemical model was used to estimate combustion complete-  
ness as well as fuel load and the associated spatial variability (van der Werf et al.,  
2006, and references therein). BC emissions were then derived from the total carbon  
emissions based on BC emission factors.

A recent study by Randerson et al. (2012) pointed out that, in the current generation  
of global burned area products (for example, the GFED), small fires had not been sys-  
tematically quantified since many of them were well below the detection limit of burned  
area. However, these fires often generated thermal anomalies that could be detected  
by satellites, such as from the MODIS active fire counts products. Burned areas in the  
GFED emissions were mainly derived from MODIS 500 m surface reflectance product,  
which could detect large fires that leave fire scars greater than 500 m or so (Giglio et  
al., 2006, 2010). In contrast, active fires, based on thermal anomalies, could detect  
fires that are an order of magnitude smaller, which may capture many aspects of the  
spatial distribution and seasonality of burning (Randerson et al., 2012 and references  
therein). As a result, active fires probably could better capturing smaller prescribed and  
agricultural fires (Randerson et al., 2012 and references therein). The active fire data  
are often used as a proxy for area burned due to the lack of long-term global burned  
area data (Giglio et al., 2006). There are many uncertainties to relate fire counts to ac-  
tual area burned due to inadequate temporal sampling, variability in fuel conditions and  
cloud cover, differences in fire behavior, and issues related to spatial resolution (Giglio  
et al., 2006; Kasischke et al., 2003). We here use MODIS active fire counts to scale  
the spatiotemporal variability of the GFEDv2 biomass burning emissions from a 3 yr  
period (2005–2007), aiming to capture some of the missing small fires. The assump-  
tion here is that burned area is proportional to fire counts. Based on this assumption,  
estimated burned areas from fire counts are relatively accurate (Giglio et al., 2006,  
2010). Since the relationship between burned area and active fires was non-linear in  
GFEDv2, the linear scale will give a different pattern of the emissions, which proba-  
bly could improve the spatiotemporal distributions of the emissions and capture some

## Top-down estimates of biomass burning emissions of black carbon

Y. H. Mao et al.

Title Page

Abstract

Introduction

Conclusions

References

Tables

Figures

⏪

⏩

◀

▶

Back

Close

Full Screen / Esc

Printer-friendly Version

Interactive Discussion







## Top-down estimates of biomass burning emissions of black carbon

Y. H. Mao et al.

Title Page

Abstract

Introduction

Conclusions

References

Tables

Figures

⏪

⏩

◀

▶

Back

Close

Full Screen / Esc

Printer-friendly Version

Interactive Discussion



OC and BC at different temperatures (Chow et al., 2004). The uncertainties of the TOR method are still difficult to quantify (Park et al., 2003; Chow et al., 1993). To linearization forward model, the Jacobian matrix  $\mathbf{K}$  ( $\mathbf{K} = \nabla_{\mathbf{x}} F$ ) is used to relate sources to concentrations in a forward model and describes the sensitivity of the measurement vector to finite change in the state vector. The forward model, in our case, GEOS-Chem provides the connection between emissions and species concentrations.  $\mathbf{K}$  is calculated by dividing the model simulated variation of BC concentrations by the perturbation of monthly mean emissions from each individual source or source region. The linear approximation of the forward model was tested by perturbing monthly mean emissions by 5 % and 10 %. We found almost linear changes of model BC concentrations resulting from perturbing the monthly mean emissions. The error vector  $\boldsymbol{\varepsilon}$ , in Eq. (1), includes contributions from errors in the observations, in the forward model, and in the model parameters. From inversion of Eq. (1), involving weighting the error statistics of  $\boldsymbol{\varepsilon}$  and  $\boldsymbol{\varepsilon}_a$  (a priori error), we can obtain an optimal solution of  $\mathbf{x}$  by given  $\mathbf{y}$  based on our prior knowledge  $\mathbf{x}_a$ .

The inverse model describes the best estimate of sources of BC, which is consistent with both the observed BC concentrations and the a priori sources of BC, given their respective uncertainties. Based on Bayes' theorem with the assumption of Gaussian error distributions, the MAP solution for  $\mathbf{x}$  by given  $\mathbf{y}$ , is equivalent to finding the minimum in the cost function  $J(\mathbf{x})$  (Rodgers, 2000):

$$J(\mathbf{x}) = (\mathbf{y} - \mathbf{K}\mathbf{x})^T \mathbf{S}_{\Sigma}^{-1} (\mathbf{y} - \mathbf{K}\mathbf{x}) + (\mathbf{x} - \mathbf{x}_a)^T \mathbf{S}_a^{-1} (\mathbf{x} - \mathbf{x}_a) \quad (2)$$

where  $\mathbf{x}_a$  and  $\mathbf{S}_a$  are the background model state vector and its associated error covariance;  $\mathbf{S}_{\Sigma}$  is the covariance of the total observational error.

Solution to  $\nabla_{\mathbf{x}} J(\mathbf{x}) = 0$  yields,

$$\hat{\mathbf{x}} = \mathbf{x}_a + (\mathbf{K}^T \mathbf{S}_{\Sigma}^{-1} \mathbf{K} + \mathbf{S}_a^{-1})^{-1} \mathbf{K}^T \mathbf{S}_{\Sigma}^{-1} (\mathbf{y} - \mathbf{K}\mathbf{x}_a) \quad (3)$$

$$\hat{\mathbf{S}} = (\mathbf{K}^T \mathbf{S}_{\Sigma}^{-1} \mathbf{K} + \mathbf{S}_a^{-1})^{-1} = (\mathbf{I} - \mathbf{A}) \mathbf{S}_a (\mathbf{I} - \mathbf{A})^T + \mathbf{G} \mathbf{S}_{\Sigma} \mathbf{G}^T \quad (4)$$



## Top-down estimates of biomass burning emissions of black carbon

Y. H. Mao et al.

Title Page

Abstract

Introduction

Conclusions

References

Tables

Figures

⏪

⏩

◀

▶

Back

Close

Full Screen / Esc

Printer-friendly Version

Interactive Discussion

sions in the Pacific Northwest (BBPNW), and anthropogenic emissions in the WUS (ANTHWUS). Figure 1 shows these three biomass burning BC source regions in the WUS. Anthropogenic emissions discussed here include both fossil fuel and biofuel emissions from Bond et al. (2007) unless stated otherwise. The averaging kernels are also useful to test the sensitivities of the inversions to the uncertainties of the observations and the a priori. The performances of the averaging kernels are discussed further in later paragraphs.

We conducted inversions with different sets of error specifications as a way to examine the sensitivities of the inversions to the a priori error and the observation error. We will discuss the error specifications in the next three paragraphs. We assumed errors of each element of state vector to be spatially uncorrelated so that background model state vector  $\mathbf{S}_a$  would be diagonal. Previously, Mao et al. (2011) found that North American anthropogenic emissions in the model were reasonably prescribed, although model was still not perfect to capture the day-to-day variabilities and magnitudes of observed surface BC concentrations at sites where North American anthropogenic emissions dominated. We thus assumed that the uncertainties of fossil fuel and biofuel emissions were 50 % in the WUS. GFED biomass burning emissions of BC were assigned an uncertainty of 300 or 500 %. Our assumption for biomass burning emissions is based on the fact that the uncertainty of BC emissions estimates generally is a factor of 2–5 on regional scales (Ramanathan and Carmichael, 2008). We also believed that GFEDv2 biomass burning emissions of BC were biased low by a factor of two in the WUS during July–October fire season of 2006 (Mao et al., 2011).

The total observation error  $\mathbf{S}_\Sigma$  includes contributions mainly from transport error in the forward model, representation error, and measurement accuracy. We estimated the transport errors by computing the variance of the relative difference between the observations and the collocated model BC concentrations (Palmer et al., 2003; Heald et al., 2004). The mean model bias, as diagnosed by the mean relative difference, is due to errors in the a priori sources and the variance of relative residual error is mainly due to errors in the transport. The calculated transport error is about 20 % in

the GEOS-Chem and consistent with previous studies (Palmer et al., 2003; Heald et al., 2004). The representation error describes the mismatch between the observations and the corresponding values simulated by the forward model. This error arises because the model only provides concentration data averaged over the grid scale which the observations do not fully cover. Representation error was about 5–10 % of the observed concentrations, by exam the statistics of the subgrid variability over the  $2^\circ \times 2.5^\circ$  GEOS-Chem model grid (Palmer et al., 2003). We assumed representation error to be 5 or 10 % following previous works. As for the instrument accuracy, uncertainties of the TOR method are difficult to quantify and no total error is prescribed for the BC measurement from the IMPROVE network (Park et al., 2003; Chow et al., 1993). We assumed the measurement error to be 5–10 %. We thus tested the total observation error  $\mathbf{S}_\Sigma$  using 30 or 50 %.

We here use the averaging kernels and the number of degrees of freedom for signal (DOFs) to test the sensitivities of the inversions to the uncertainties of the a priori and the inversion system. DOFs is the trace of the averaging kernel matrix (Rodger, 2000). The number of pieces of information from a perfect knowledge of the observing system has an expected value of the size of the state vector. DOFs thus is expected to be close to 4 in our case. Table 1 compares the DOFs from inversions using different error specifications as well as at two different model horizontal resolutions. By inspecting averaging kernels (not shown) and DOFs (Table 1), we considered the best inversions as those with error specifications of 500 % for the a priori biomass burning emissions and 30 % for the observations. The inversions with this set of error specifications show better performance of averaging kernels (Fig. 6) and higher values of DOFs (closer to four; bottom two rows in Table 1). Figure 6 compares the averaging kernels for the inversions of BC sources for May–October 2006, using GEOS-Chem at  $2^\circ \times 2.5^\circ$  and  $0.5^\circ \times 0.667^\circ$  horizontal resolutions and with aforementioned best set of error characterizations (bottom two rows in Table 1). Individual lines here are corresponding to the individual rows of averaging kernel matrix  $\mathbf{A}$ . Red line for example, it is the sensitivity of the a posteriori emissions in California and the Southwest to the unknown true state, which shows

## Top-down estimates of biomass burning emissions of black carbon

Y. H. Mao et al.

[Title Page](#)[Abstract](#)[Introduction](#)[Conclusions](#)[References](#)[Tables](#)[Figures](#)[Back](#)[Close](#)[Full Screen / Esc](#)[Printer-friendly Version](#)[Interactive Discussion](#)

## Top-down estimates of biomass burning emissions of black carbon

Y. H. Mao et al.

Title Page

Abstract

Introduction

Conclusions

References

Tables

Figures

⏪

⏩

◀

▶

Back

Close

Full Screen / Esc

Printer-friendly Version

Interactive Discussion

that inversion system has enough information to constrain the biomass burning emissions in California and the Southwest uniquely, especially during July to September. Generally, our inversion system could largely constrain the four elements of the state vector independently, especially during July to September and to a less degree in October. Anthropogenic emissions in the WUS could not be separated completely from the three biomass burning emissions elements in May and June. We also compared the averaging kernels and DOFs at different model resolutions. Averaging kernels at both two model resolutions show similar performances, which indicate that inversion system can largely constrain the four elements of state vector independently. DOFs also have acceptable values for inversions at both two resolution models (Table 1). We thus believe our error specifications are appropriate. The retrieval at  $0.5^\circ \times 0.667^\circ$  horizontal resolution is better constrained by the observation system, which shows better performance of averaging kernels and higher DOFs values (bottom row in Table 1). Further discussion about the inversions with different set of error characterizations and at different model horizontal resolutions are presented in Sect. 5.1 (Fig. 7). The sensitivity of the a posteriori solutions to the assumed uncertainties is also assessed in Sect. 5.1.1. We evaluate a posteriori estimates in Sect. 5.1.3. More discussions about the sensitivity of model resolution to the retrieval are presented in Sect. 5.2.

## 5 Inversion results and discussions

### 5.1 A posteriori estimates of BC emissions

#### 5.1.1 Comparisons with a priori emissions

Figure 7 shows the a priori and the a posteriori estimates of monthly BC emissions in the WUS for May–October 2006. For the purpose of clarity, anthropogenic emissions are divided by three in the figures to be compatible with the magnitude of the biomass burning emissions. Error bars here represent uncertainties of the emissions.

## Top-down estimates of biomass burning emissions of black carbon

Y. H. Mao et al.

Title Page

Abstract

Introduction

Conclusions

References

Tables

Figures

⏪

⏩

◀

▶

Back

Close

Full Screen / Esc

Printer-friendly Version

Interactive Discussion

The a posteriori estimates of BC sources are from several sensitivity experiments discussed in Sect. 4 (Table 1). Those experiments include inversions using different sets of error specifications, with 300 or 500 % for the uncertainties of the a priori biomass burning emissions and with 30 or 50 % for the observational error, and at  $2^\circ \times 2.5^\circ$  or  $0.5^\circ \times 0.667^\circ$  two different model horizontal resolutions. The cost functions reduce by  $\sim 40\%$  after inversions in those experiments. The BC emissions after inversions with different error specifications show similar trend. The a posteriori biomass burning emissions increase dramatically and consistently (about a factor of 3–5 on average) while the a posteriori anthropogenic emissions reduce substantially ( $\sim 50\%$ ). Detailed analyses are in Table 2 and discussed in the following paragraph. Our retrievals also largely reduce the uncertainties of the emissions, which decline by at least 50 % or by even larger than 90 %. Those sensitivity experiments thus reflect that our retrievals are reliable. We consider the best retrievals as those with 500 % for the error of a priori biomass burning emissions and 30 % for the total observational error. The best retrievals include relatively small uncertainties of the a posteriori. The estimates are also consistent with our discussion in Sect. 4, which shows that the inversions with this set of error specifications provide largest DOFs values (Table 1) as well as best performance of the averaging kernels. The inversion at  $0.5^\circ \times 0.667^\circ$  horizontal resolution with best error specifications show smallest uncertainties of the a posteriori emissions, which again is consistent with analyses based on Table 1 and Fig. 6. This implies that inversion at  $0.5^\circ \times 0.667^\circ$  horizontal resolution with errors of 500 % for the a priori biomass burning emissions and 30 % for the observations provides the best estimates. This inversion is further confirmed to be the best one by analyzing resulting model surface BC concentrations both in the Sect. 5.1.3 and in Sect. 5.3. In the following text, our discussion about the a posteriori estimates of BC emissions and the resulting surface BC concentrations are thus based on the retrievals with aforementioned error specifications. For further evaluation, we summarize the monthly BC emissions of a priori and a posteriori estimates from the best inversions in the following paragraph.

## Top-down estimates of biomass burning emissions of black carbon

Y. H. Mao et al.

Title Page

Abstract

Introduction

Conclusions

References

Tables

Figures

⏪

⏩

◀

▶

Back

Close

Full Screen / Esc

Printer-friendly Version

Interactive Discussion

Table 2 compares monthly biomass burning BC emissions from the three regions in the WUS and anthropogenic BC emissions over the WUS before and after retrievals for May–October 2006. The a priori GFEDv2 and the a posteriori biomass burning BC emissions are from inversions at  $2^\circ \times 2.5^\circ$  and  $0.5^\circ \times 0.667^\circ$  horizontal resolutions.

In general, the a posteriori biomass burning emissions increase by factors of 4.7 at  $2^\circ \times 2.5^\circ$  and 2.8 at  $0.5^\circ \times 0.667^\circ$  horizontal resolutions in the WUS during July to September, compared with a priori emissions. The a posteriori biomass burning emissions also show large variations from month to month, at different source regions and at different model horizontal resolutions. For example, the biomass burning emissions of BC after retrieval at  $2^\circ \times 2.5^\circ$  horizontal resolution during July to September are 6.0 and 3.3 times higher than the a priori GFEDv2 in the Rockies and in California and the Southwest, respectively. Monthly biomass burning emissions at  $2^\circ \times 2.5^\circ$  horizontal resolution in the WUS may increase by factors of 6.3 in July and 3.6 in August; the correspondingly values are 4.1 and 2.2, respectively, at  $0.5^\circ \times 0.667^\circ$  horizontal resolutions. More discussions about the sensitivity of the retrieval to model resolution are presented in the Sect. 5.2. The a posteriori anthropogenic emissions in the WUS decrease by 48 % from the inversion at  $2^\circ \times 2.5^\circ$  and by 36 % at  $0.5^\circ \times 0.667^\circ$  for May–October 2006 compared to 2000 level (Bond et al., 2007). This decreasing trend of anthropogenic emissions estimates is consistent with the study by Rao and Somers (2010), which found that BC emissions in the US had declined by about 30 % from 1990 to 2005 and were expected to decline by an additional 80 % by 2030 compared to 2005 level. Observed BC concentrations from 50 IMPROVE sites in the US also decreased by over 25 % on average from 1990 to 2004, which also implies that emission control have been effective in reducing BC across US (Murphy et al., 2011).

### 5.1.2 Comparisons with GFEDv3 and FLAMBE

Monthly BC emissions from GFEDv3 (van derWerf et al., 2010) and the Fire Locating and Monitoring of Burning Emissions (FLAMBE) inventory (Reid et al., 2009) are calculated over three biomass burning regions for May–October 2006 and compared with a



estimates, GFEDv3 emissions of BC in the WUS are still biased low by factors of 4.4 at  $2^\circ \times 2.5^\circ$  and 2.7 at  $0.5^\circ \times 0.667^\circ$  for July–September 2006. FLAMBE BC emissions in the WUS are much higher than the a priori GFED emissions (a factor of 5.9) and even the a posteriori estimates (factors of 1.3 at  $2^\circ \times 2.5^\circ$  and 2.1 at  $0.5^\circ \times 0.667^\circ$ ) during July–September 2006. FLAMBE may cover more small fire events due to its hourly temporal resolution. However, simulated BC concentrations with FLAMBE emissions are still problematic and cannot capture the temporal variations of observations well (not shown). Model simulations with FLAMBE also show false high fire contributions to surface BC concentrations, which implies that FLAMBE might be systematically too high. Our analyses are in agreement with previous studies by Wang et al. (2011) and Fisher et al. (2010), which suggested that FLAMBE needed to be reduced to 53% in Russian and 45% in the Southeast Asian, respectively, when simulated CO, BC and OC with GEOS-Chem for the NASA Arctic Research of the Composition of the Troposphere from Aircraft and Satellites (ARCTAS) (Jacob et al., 2010) and the NOAA Aerosol, Radiation and Cloud Processes affecting Arctic Climate (ARCPAC) (Brock et al., 2011) campaigns.

### 5.1.3 Evaluation a posteriori estimates with IMPROVE observations

Figures 8–10 compare the observed and simulated surface BC concentrations at selective IMPROVE sites in the Rockies (Fig. 8), in the Pacific Northwest (Fig. 9), and in California and the Southwest (Fig. 10), respectively. Model results shown here are from the simulations with the standard GFEDv2 8-day emissions at  $2^\circ \times 2.5^\circ$  horizontal resolution and with the a posteriori estimates at both  $2^\circ \times 2.5^\circ$  and  $0.5^\circ \times 0.667^\circ$  horizontal resolutions for May–October 2006. Model simulated surface BC concentrations with the a posteriori emissions show significant enhancements for July–September 2006. Model surface BC after inversions can capture the major fire episodes at many IMPROVES sites. Here shown some representative sites in the three regions over the WUS. Model surface BC concentrations with the a posteriori estimates show better agreement with IMPROVE observations, which largely reproduce both synoptic vari-

## Top-down estimates of biomass burning emissions of black carbon

Y. H. Mao et al.

Title Page

Abstract

Introduction

Conclusions

References

Tables

Figures



Back

Close

Full Screen / Esc

Printer-friendly Version

Interactive Discussion



ability and magnitude of the observed surface BC concentrations. Detailed statistic analyses are in Sect. 5.3. Discussions about the sensitivity of the retrieval to model resolution are presented in Sect. 5.2.

Figure 11 compares the observed and simulated surface BC concentrations averaged for sites in the Rockies, in California and the Southwest, and in the Pacific Northwest, respectively. Model simulations are same as those in Figs. 8–10. Again, Fig. 11 shows significantly increased model surface BC concentrations with the a posteriori emissions for July–September 2006, especially in the Rockies (up to  $\sim 100\%$  increase) and to a less degree in the Pacific Northwest (up to  $\sim 50\%$  increase). These improved comparisons between simulated surface BC concentrations and the observations in the Rockies may be due to the largest enhancement of biomass burning emissions after inversions. Model simulated surface BC concentrations averaged for sites in California and the Southwest show slight increase compared with those averaged in the other two regions, which may be due to the fact that most of IMPROVE sites in California and the Southwest are not located at the regions with large fires.

Figure 12 compares the observed and model simulated daily surface BC concentrations for May–October 2006, averaged for sites at the altitude ranges 0–1, 1–2, 2–3, and 3–4 km, respectively. Model simulations again are same as those in Figs. 8–10. Model simulated surface BC concentrations with the a posteriori emissions show substantial enhancements at all altitude ranges, especially at the 1–2 (up to  $0.18\ \mu\text{g m}^{-3}$  increase) and 2–3 km (up to  $0.11\ \mu\text{g m}^{-3}$  increase) altitude ranges. There are also some improvements in late June 2006 (up to  $0.06\ \mu\text{g m}^{-3}$  at the 2–3 km altitude range), which may partially verify our aforementioned adjustment using the MODIS fire counts to improve the spatiotemporal distributions of the GFED emissions. Our previous study by Mao et al. (2011) showed that simulated BC concentrations were biased low by a factor of two at elevated mountainous sites during the July–October 2006. The a posteriori emissions lead to an average bias reduction of  $\sim 50\%$  in the simulated surface BC concentrations at the 1–2 km altitude range. As widely pointed out in previous studies, part of the discrepancies is because of the model resolution, which is too coarse to

## Top-down estimates of biomass burning emissions of black carbon

Y. H. Mao et al.

Title Page

Abstract

Introduction

Conclusions

References

Tables

Figures

⏪

⏩

◀

▶

Back

Close

Full Screen / Esc

Printer-friendly Version

Interactive Discussion







the azimuthal angle, and the centered RMS error difference between a simulated field and the reference data is proportional to the distance between these two points (i.e., the closer a model is to the observational point, the lower its centered RMS error).

Taylor skill score is defined by,

$$S = \frac{4(1 + R)}{(\frac{\sigma_f}{\sigma_r} + \frac{\sigma_r}{\sigma_f})^2(1 + R_0)} \quad (6)$$

Where  $R$  is the correlation coefficient between  $f$  and  $r$ ;  $\sigma_f$  and  $\sigma_r$  are the standard deviations of  $f$  and  $r$ ;  $R_0$  is the maximum correlation attainable. As the model variance approached the observed variance,  $\sigma_f/\sigma_r \rightarrow 1$ ,  $R \rightarrow R_0$  and skill score approached unity. Under this definition, skill score increases toward value 1 as the correlation becomes larger and larger or as the model variance approaches the observed variance. Model simulation thus shows better performance with higher skill score.

We use Taylor diagrams in Fig. 13 to compare the correlation coefficients, the standard deviations, and the centered RMS error of simulated and observed BC concentrations averaged for 69 IMPROVE sites. Taylor diagram in Fig. 14 is same as Fig. 13 but for 69 individual sites. Model standard deviations and centered RMS error for each site are normalized by observed standard deviation at that site in Fig. 14. Three indexes, correlation coefficients, standard deviations and centered RMS error, consistently show that model simulated surface BC concentrations with the a posteriori emissions are in better agreement with the observations, especially using the nested model. Averaged correlation coefficient for all 69 sites increases from 0.28 with the standard GFEDv2 emissions to 0.36 with the a posteriori estimates (Fig. 13). Our retrievals also largely improve the dispersion of the model BC concentrations. Standard deviations after inversions at two different resolutions are closer to that of the observations. The averaged standard deviations with the a posteriori emissions increase from 0.11 to 0.16 at  $2^\circ \times 2.5^\circ$  and to 0.19 at  $0.5^\circ \times 0.667^\circ$ . The centered RMS after the retrievals are also lower, which again implies that model simulated surface BC concentrations using the a posteriori estimates are closer to the observations. With the a posteriori emis-

Top-down estimates of biomass burning emissions of black carbon

Y. H. Mao et al.

Title Page

Abstract

Introduction

Conclusions

References

Tables

Figures

⏪

⏩

◀

▶

Back

Close

Full Screen / Esc

Printer-friendly Version

Interactive Discussion





**Top-down estimates  
of biomass burning  
emissions of black  
carbon**

Y. H. Mao et al.

Title Page

Abstract

Introduction

Conclusions

References

Tables

Figures

⏪

⏩

◀

▶

Back

Close

Full Screen / Esc

Printer-friendly Version

Interactive Discussion

as the a posteriori biomass burning emissions increased by factors of 4.7 and 2.8, respectively, relative to the a priori emissions during July to September 2006. The a posteriori biomass burning emissions also showed large variations from month to month, at different source regions, and at different model horizontal resolutions. The a posteriori biomass burning emissions increase less at  $0.5^\circ \times 0.667^\circ$  than those at  $2^\circ \times 2.5^\circ$ . The large differences in the a posteriori emissions at the two model horizontal resolutions were likely due to the better simulated boundary layer and more concentrated emissions in the nested model.

Compared with a priori emissions in the WUS during July to September 2006, the GFEDv3 BC emissions increased by 8% in the WUS, especially evident in August (20%) and September 2006 (15%); while FLAMBE BC emissions were higher by a factor of 5.9. Compared with the a posteriori estimates, GFEDv3 emissions of BC in the WUS were still biased low by factors of 4.4 at  $2^\circ \times 2.5^\circ$  and 2.7 at  $0.5^\circ \times 0.667^\circ$  for July–September 2006; while FLAMEB were higher by factors of 1.3 and 2.1, respectively. However, FLAMBE emissions might be systematically too high and problematic in its temporal variations.

Model surface BC with the a posteriori emissions captured the major fire episodes at many IMPROVE sites, especially at the 1–2 and 2–3 km altitude ranges. Model surface BC concentrations with the a posteriori estimates provided better agreement with IMPROVE observations for July–September 2006, especially in the Rockies and to a less degree in the Pacific Northwest. With the a posteriori emissions, the resulting Taylor skill scores increased by 86% at  $2^\circ \times 2.5^\circ$  and by 132% at  $0.5^\circ \times 0.667^\circ$  horizontal resolutions. Model BC concentrations at two different resolutions also showed largest differences during July to September. The a posteriori emissions led to a bias reduction of  $\sim 50\%$  on average in the simulated surface BC concentrations.

*Acknowledgements.* This research was supported by NASA grant NNX09AF07G from the Atmospheric Chemistry Modeling and Analysis Program (ACMAP). The GEOS-Chem model is managed by the Atmospheric Chemistry Modeling group at Harvard University with support





**Top-down estimates  
of biomass burning  
emissions of black  
carbon**

Y. H. Mao et al.

Title Page

Abstract

Introduction

Conclusions

References

Tables

Figures

◀

▶

◀

▶

Back

Close

Full Screen / Esc

Printer-friendly Version

Interactive Discussion

- Cooke, W. F., Lioussé, C., Cachier, H., and Feichter, J.: Construction of a 1° × 1° fossil fuel emission data set for carbonaceous aerosol and implementation and radiative impact in the ECHAM4 model, *J. Geophys. Res.*, 104, 22137–22162, 1999.
- Fairlie, T. D., Jacob, D. J., and Park, R. J.: The impact of transpacific transport of mineral dust in the United States, *Atmos. Environ.*, 41, 1251–1266, 2007.
- Fisher, J. A., Jacob, D. J., Purdy, M. T., Kopacz, M., Le Sager, P., Carouge, C., Holmes, C. D., Yantosca, R. M., Batchelor, R. L., Strong, K., Diskin, G. S., Fuelberg, H. E., Holloway, J. S., Hyer, E. J., McMillan, W. W., Warner, J., Streets, D. G., Zhang, Q., Wang, Y., and Wu, S.: Source attribution and interannual variability of Arctic pollution in spring constrained by aircraft (ARCTAS, ARCPAC) and satellite (AIRS) observations of carbon monoxide, *Atmos. Chem. Phys.*, 10, 977–996, doi:10.5194/acp-10-977-2010, 2010.
- Flanner, M. G., Zender, C. S., Randerson, J. T., and Rasch, P. J.: Present-day climate forcing and response from black carbon in snow, *J. Geophys. Res.*, 112, D11202, doi:10.1029/2006JD008003, 2007.
- Flanner, M. G., Zender, C. S., Hess, P. G., Mahowald, N. M., Painter, T. H., Ramanathan, V., and Rasch, P. J.: Springtime warming and reduced snow cover from carbonaceous particles, *Atmos. Chem. Phys.*, 9, 2481–2497, doi:10.5194/acp-9-2481-2009, 2009.
- Fuglestad, J. S., Shine, K. P., Bernsten, T., Cook, J., Lee, D. S., Stenke, A., Skeie, R. B., Velders, G. J. M., and Waitz, I. A.: Transport impacts on atmosphere and climate: Metrics, *Atmos. Environ.*, 44, 4648–4677, 2010.
- Giglio, L., van der Werf, G. R., Randerson, J. T., Collatz, G. J., and Kasibhatla, P.: Global estimation of burned area using MODIS active fire observations, *Atmos. Chem. Phys.*, 6, 957–974, doi:10.5194/acp-6-957-2006, 2006.
- Giglio, L., Randerson, J. T., van der Werf, G. R., Kasibhatla, P. S., Collatz, G. J., Morton, D. C., and DeFries, R. S.: Assessing variability and long-term trends in burned area by merging multiple satellite fire products, *Biogeosciences*, 7, 1171–1186, doi:10.5194/bg-7-1171-2010, 2010.
- Gleckler, P. J., Taylor, K. E., and Doutriaux, C.: Performance metrics for climate models, *J. Geophys. Res.*, 113, D06104, doi:10.1029/2007JD008972, 2008.
- Hansen, J. and Nazarenko, L.: Soot climate forcing via snow and ice albedos, *P. Natl. Acad. Sci. USA*, 101, 423–428, 2004.
- Hansen, J., Sato, M., Ruedy, R., Nazarenko, L., Lacis, A., Schmidt, G. A., Russell, G., Aleinov, I., Bauer, M., Bauer, S., Bell, N., Cairns, B., Canuto, V., Chandler, M., Cheng, Y., Del Genio,

## Top-down estimates of biomass burning emissions of black carbon

Y. H. Mao et al.

Title Page

Abstract

Introduction

Conclusions

References

Tables

Figures

⏪

⏩

◀

▶

Back

Close

Full Screen / Esc

Printer-friendly Version

Interactive Discussion

A., Faluvegi, G., Fleming, E., Friend, A., Hall, T., Jackman, C., Kelley, M., Kiang, N., Koch, D., Lean, J., Lerner, J., Lo, K., Menon, S., Miller, R., Minnis, P., Novakov, T., Oinas, V., Perlwitz, Ja., Perlwitz, Ju., Rind, D., Romanou, A., Shindell, D., Stone, P., Sun, S., Tausnev, N., Thresher, D., Wielicki, B., Wong, T., Yao, M., and Zhang, S.: Efficacy of climate forcings, J. Geophys. Res., 110, D18104, doi:10.1029/2005JD005776, 2005.

Heald, C. L., Jacob, D. J., Jones, D. B. A., Palmer, P. I., Logan, J. A., Streets, D. G., Sachse, G. W., Gille, J. C., Hoffman, R. N., and Nehr Korn, T.: Comparative inverse analysis of satellite (MOPITT) and aircraft (TRACE-P) observations to estimate Asian sources of carbon monoxide, J. Geophys. Res., 109, D15S04, doi:10.1029/2004JD005185, 2004.

Horvath, H.: Atmospheric light absorption – a review, Atmos. Environ., 27, 293–317, 1993.

Intergovernmental Panel on Climate Change (IPCC): The Physical Science Basis, Contribution of Working Group I to the Fourth Assessment Report of the Intergovernmental Panel on Climate Change, edited by: Solomon, S., Qin, D., Manning, M., Chen, Z., Marquis, M., Averyt, K. B., Tignor, M., and Miller, H. L., Cambridge Univ. Press, Cambridge, UK, 2007.

Jacob, D. J., Crawford, J. H., Maring, H., Clarke, A. D., Dibb, J. E., Emmons, L. K., Ferrare, R. A., Hostetler, C. A., Russell, P. B., Singh, H. B., Thompson, A. M., Shaw, G. E., McCauley, E., Pederson, J. R., and Fisher, J. A.: The Arctic Research of the Composition of the Troposphere from Aircraft and Satellites (ARCTAS) mission: design, execution, and first results, Atmos. Chem. Phys., 10, 5191–5212, doi:10.5194/acp-10-5191-2010, 2010.

Jacobson, M. Z.: Strong radiative heating due to the mixing state of black carbon in atmospheric aerosols, Nature, 409, 695–697, 2001.

Jacobson, M. Z.: Control of fossil-fuel particulate black carbon and organic matter, possibly the most effective method of slowing global warming, J. Geophys. Res., 107, 4410, doi:10.1029/2001JD001376, 2002.

Jacobson, M. Z.: Climate response of fossil fuel and biofuel soot, accounting for soot's feedback to snow and sea ice albedo and emissivity, J. Geophys. Res., 109, D21201, doi:10.1029/2004JD004945, 2004.

Jacobson, M. Z.: Short-term effects of controlling fossil-fuel soot, biofuel soot and gases, and methane on climate, Arctic ice, and air pollution health, J. Geophys. Res., 115, D14209, doi:10.1029/2009JD013795, 2010.

Jaffe, D., Hafner, W., Chand, D., Westerling, A., and Spracklen, D.: Interannual variations in PM<sub>2.5</sub> due to wildfires in the western United States, Environ. Sci. Technol., 42, 2812–2818, 2008.

**Top-down estimates  
of biomass burning  
emissions of black  
carbon**

Y. H. Mao et al.

Title Page

Abstract

Introduction

Conclusions

References

Tables

Figures

◀

▶

◀

▶

Back

Close

Full Screen / Esc

Printer-friendly Version

Interactive Discussion

- Jiang, Z., Jones, D. B. A., Kopacz, M., Liu, J., Henze, D. K., and Heald, C.: Quantifying the impact of model errors on top-down estimates of carbon monoxide emissions using satellite observations, *J. Geophys. Res.*, 116, D15306, doi:10.1029/2010JD015282, 2011.
- Jones, D. B. A., Bowman, K. W., Logan, J. A., Heald, C. L., Liu, J., Luo, M., Worden, J., and Drummond, J.: The zonal structure of tropical O<sub>3</sub> and CO as observed by the Tropospheric Emission Spectrometer in November 2004 – Part 1: Inverse modeling of CO emissions, *Atmos. Chem. Phys.*, 9, 3547–3562, doi:10.5194/acp-9-3547-2009, 2009.
- Kasibhatla, P., Arellano, A., Logan, J. A., Palmer, P. I., and Novelli, P.: Top-down estimate of a large source of atmospheric carbon monoxide associated with fuel combustion in Asia, *Geophys. Res. Lett.*, 29, L191900, doi:10.1029/2002GL015581, 2002.
- Kasischke, E. S., Hewson, J. H., Stocks, B., van der Werf, G., and Randerson, J.: The use of ATSR active fire counts for estimating relative patterns of biomass burning – a study from the boreal forest region, *Geophys. Res. Lett.*, 30, doi:10.1029/2003GL017859, 2003.
- Koch, D., Bond, T. C., Streets, D., Unger, N., and van der Werf, G. R.: Global impacts of aerosols from particular source regions and sectors, *J. Geophys. Res.*, 112, D02205, doi:10.1029/2005JD007024, 2007.
- Kopacz, M., Jacob, D. J., Henze, D. K., Heald, C. L., Streets, D. G., and Zhang, Q.: Comparison of adjoint and analytical Bayesian inversion methods for constraining Asian sources of carbon monoxide using satellite (MOPITT) measurements of CO columns, *J. Geophys. Res.*, 114, D04305, doi:10.1029/2007JD009264, 2009.
- Kopp, R. E. and Mauzerall, D. L.: Assessing the climatic benefits of black carbon mitigation, *P. Natl. Acad. Sci. USA*, 26, 11703–11708, 2010.
- Korontzi, S., McCarty, J., Loboda, T., Kumar, S., and Justice, C.: Global distribution of agricultural fires in croplands from 3 years of Moderate Resolution Imaging Spectroradiometer (MODIS) data, *Global Biogeochem. Cy.*, 20, GB2021, doi:10.1029/2005GB002529, 2006.
- Langmann, B., Duncan, B., Textor, C., Trentmann, J., van der Werf, G. R.: Vegetation fire emissions and their impact on air pollution and climate, *Atmos. Environ.*, 43, 107–116, 2009.
- Levy II, H., Schwarzkopf, M. D., Horowitz, L., Ramaswamy, V., and Findell, K. L.: Strong sensitivity of late 21st century climate to projected changes in short-lived air pollutants, *J. Geophys. Res.*, 113, D06102, doi:10.1029/2007JD009176, 2008.
- Liu, H., Jacob, D. J., Bey, I., and Yantosca, R. M.: Constraints from <sup>210</sup>Pb and <sup>7</sup>Be on wet deposition and transport in a global three-dimensional chemical tracer model driven by assimilated meteorological fields, *J. Geophys. Res.*, 106, 12109–12128, 2001.

**Top-down estimates  
of biomass burning  
emissions of black  
carbon**

Y. H. Mao et al.

Title Page

Abstract

Introduction

Conclusions

References

Tables

Figures

◀

▶

◀

▶

Back

Close

Full Screen / Esc

Printer-friendly Version

Interactive Discussion

- Mao, Y. H., Li, Q. B., Zhang, L., Chen, Y., Randerson, J. T., Chen, D., and Liou, K. N.: Biomass burning contribution to black carbon in the Western United States Mountain Ranges, *Atmos. Chem. Phys.*, 11, 11253–11266, doi:10.5194/acp-11-11253-2011, 2011.
- Malm, W. C., Sisler, J. F., Huffman, D., Eldred, R. A., and Cahill, T. A.: Spatial and seasonal trends in particle concentration and optical extinction in the United States, *J. Geophys. Res.*, 99, 1347–1370, 1994.
- McCarty, J. L., Korontzi, S., Justice, C. O., and Loboda, T.: The spatial and temporal distribution of crop residue burning in the contiguous United States, *Sci. Total Environ.*, 407, 5701–5712, doi:10.1016/j.scitotenv.2009.07.009, 2009.
- Murphy, D. M., Chow, J. C., Leibensperger, E. M., Malm, W. C., Pitchford, M., Schichtel, B. A., Watson, J. G., and White, W. H.: Decreases in elemental carbon and fine particle mass in the United States, *Atmos. Chem. Phys.*, 11, 4679–4686, doi:10.5194/acp-11-4679-2011, 2011.
- Park, R. J., Jacob, D. J., Chin, M., and Martin, R. V.: Sources of carbonaceous aerosols over the United States and implications for natural visibility, *J. Geophys. Res.*, 108, D124355, doi:10.1029/2002JD003190, 2003.
- Palmer, P. I., Jacob, D. J., Jones, D. B. A., Heald, C. L., Yantosca, R. M., Logan, J. A., Sachse, G. W., and Streets, D. G.: Inverting for emissions of carbon monoxide from Asia using aircraft observations over the western Pacific, *J. Geophys. Res.*, 108, D218828, doi:10.1029/2003JD003397, 2003.
- Palmer, P. I., Suntharalingam, P., Jones, D. B. A., Jacob, D. J., Streets, D. G., Fu, Q. Y., Vay, S. A., and Sachse, G. W.: Using CO<sub>2</sub>: CO correlations to improve inverse analyses of carbon fluxes, *J. Geophys. Res.*, 111, D12318, doi:10.1029/2005JD006697, 2006.
- Ramana, M. V., Ramanathan, V., Feng, Y., Yoon, S.-C., Kim, S.-W., Carmichael, G. R., and Schauer, J. J.: Warming influenced by the ratio of black carbon to sulphate and the black-carbon source, *Nat. Geosci.*, 3, 542–545, 2010.
- Ramanathan, V. and Carmichael, G.: Global and regional climate changes due to black carbon, *Nat. Geosci.*, 1, 221–227, 2008.
- Randerson, J. T., van der Werf, G. R., Giglio, L., Collatz, G. J., and Kasibhatla, P. S.: Global Fire Emissions Database, Version 2 (GFEDv2) (<http://daac.ornl.gov/>), Oak Ridge National Laboratory Distributed Active Archive Center, Oak Ridge, Tennessee, USA, 2007.
- Randerson, J. T., Chen, Y., van der Werf, G. R., Rogers, B. M., and Morton, D. C.: Global burned area and biomass burning emissions from small fires, *J. Geophys. Res.*, 117, G04012, doi:10.1029/2012JG002128, 2012.

## Top-down estimates of biomass burning emissions of black carbon

Y. H. Mao et al.

Title Page

Abstract

Introduction

Conclusions

References

Tables

Figures

⏪

⏩

◀

▶

Back

Close

Full Screen / Esc

Printer-friendly Version

Interactive Discussion

Rao, V. and Somers, J. H.: Black Carbon as a Short-Lived Climate Forcer: A Profile of Emission Sources and CO-Emitted Pollutants, 19th Annual International Emission Inventory Conference, San Antonio, Texas, September, 2010.

Reddy, M. S. and Boucher, O.: Climate impact of black carbon emitted from energy consumption in the world's regions, *Geophys. Res. Lett.*, 34, L11802, doi:10.1029/2006GL028904, 2007.

Reid, J. S., Hyer, E. J., Prins, E. M., Westphal, D. L., Zhang, J., Wang, J., Christopher, S. A., Curtis, C. A., Schmidt, C. C., Eleuterio, D. P., Richardson, K. A., and Hoffman, J. P.: Global monitoring and forecasting of biomass-burning smoke: description and lessons from the Fire Locating and Modeling of Burning Emissions (FLAMBE) program, *IEEE J. Sel. Top. Appl.*, 2, 144–162, doi:10.1109/JSTARS.2009.2027443, 2009.

Rodgers, C. D.: *Inverse Methods for Atmospheric Sounding: Theory and Practice*, World Sci., Singapore, 2000.

Roy, D. P. and Boschetti, L.: Southern Africa validation of the MODIS, L3JRC, and GlobCarbon burned-area products, *IEEE T. Geosci. Remote*, 47, 1032–1044, doi:10.1109/TGRS.2008.2009000, 2009.

Shindell, D. T., Levy II, H., Schwarzkopf, M. D., Horowitz, L. W., Lamarque, J.-F., and Faluvegi, G.: Multimodel projections of climate change from short-lived emissions due to human activities, *J. Geophys. Res.*, 113, D11109, doi:10.1029/2007JD009152, 2008.

Shindell, D., Kuylenstierna, J. C. I., Vignati, E., van Dingenen, R., Amann, M., Klimont, Z., Anenberg, S. C., Muller, N., Janssens-Maenhout, G., Raes, F., Schwartz, J., Faluvegi, G., Pozzoli, L., Kupiainen, K., Höglund-Isaksson, L., Emberson, L., Streets, D., Ramanathan, V., Hicks, K., Kim Oanh, N. T., Milly, G., Williams, M., Demkine, V., and Fowler, D.: Simultaneously mitigating near-term climate change and improving human health and food security, *Sciences*, 335, 183–189, 2012.

Smith, K. R., Jerrett, M., Anderson, H. R., Burnett, R. T., Stone, V., Derwent, R., Atkinson, R. W., Cohen, A., Shonkoff, S. B., Krewski, D., Pope III, C. A., Thun, M. J., and Thurston, G.: Public health benefits of strategies to reduce greenhouse-gas emissions: health implications of short-lived greenhouse pollutants, *Lancet*, 374, 2091–2103, 2009.

Streets, D. G., Gupta, S., Waldhoff, S. T., Wang, M. Q., Bond, T. C., and Bo, Y.: Black carbon emissions in China, *Atmos. Environ.*, 35, 4281–4296, 2001.

Streets, D. G., Bond, T. C., Carmichael, G. R., Fernandes, S. D., Fu, Q., He, D., Klimont, Z., Nelson, S. M., Tsai, N. Y., Wang, M. Q., Woo, J.-H., and Yarber, K. F.: An inventory of gaseous

## Top-down estimates of biomass burning emissions of black carbon

Y. H. Mao et al.

Title Page

Abstract

Introduction

Conclusions

References

Tables

Figures

⏪

⏩

◀

▶

Back

Close

Full Screen / Esc

Printer-friendly Version

Interactive Discussion

and primary aerosol emissions in Asia in the year 2000, *J. Geophys. Res.*, 108, D218809, doi:10.1029/2002JD003093, 2003.

Taylor, K. E.: Summarizing multiple aspects of model performance in a single diagram, *J. Geophys. Res.*, 106, 7183–7192, 2001.

5 van der Werf, G. R., Randerson, J. T., Giglio, L., Collatz, G. J., Kasibhatla, P. S., and Arellano Jr., A. F.: Interannual variability in global biomass burning emissions from 1997 to 2004, *Atmos. Chem. Phys.*, 6, 3423–3441, doi:10.5194/acp-6-3423-2006, 2006.

10 van der Werf, G. R., Randerson, J. T., Giglio, L., Collatz, G. J., Mu, M., Kasibhatla, P. S., Morton, D. C., DeFries, R. S., Jin, Y., and van Leeuwen, T. T.: Global fire emissions and the contribution of deforestation, savanna, forest, agricultural, and peat fires (1997–2009), *Atmos. Chem. Phys.*, 10, 11707–11735, doi:10.5194/acp-10-11707-2010, 2010.

Walcek, C. J., Brost, R. A., and Chang, J. S.: SO<sub>2</sub>, sulfate and HNO<sub>3</sub> deposition velocities computed using regional landuse and meteorological data, *Atmos. Environ.*, 20, 949–964, 1986.

15 Wang, Q., Jacob, D. J., Fisher, J. A., Mao, J., Leibensperger, E. M., Carouge, C. C., Le Sager, P., Kondo, Y., Jimenez, J. L., Cubison, M. J., and Doherty, S. J.: Sources of carbonaceous aerosols and deposited black carbon in the Arctic in winter-spring: implications for radiative forcing, *Atmos. Chem. Phys.*, 11, 12453–12473, doi:10.5194/acp-11-12453-2011, 2011.

20 Wang, Y., McElroy, M. B., Jacob, D., and Yantosca, R. M.: A nested grid formulation for chemical transport over Asia: applications to CO, *J. Geophys. Res.*, 109, D22307, doi:10.1029/2004JD005237, 2004.

Zwally, H. J., Abdalati, W., Herring, T., Larson, K., Saba, J., and Steffen, K.: Surface melt-induced acceleration of Greenland ice-sheet flow, *Science*, 297, 218–222, 2002.

## Top-down estimates of biomass burning emissions of black carbon

Y. H. Mao et al.

**Table 1.** Number of degrees of freedom for signal (DOFs) for inversions (May–October 2006) using different error characterizations and at different model horizontal resolutions.

Model resolution	Error specification	DOFs					
		May	Jun	Jul	Aug	Sep	Oct
2° × 2.5°	$S_{\Sigma} = 50\%$ $S_a \text{ BB} = 300\%$	2.36	2.68	3.60	3.85	3.81	2.99
	$S_{\Sigma} = 30\%$ $S_a \text{ BB} = 300\%$	2.87	2.80	3.80	3.93	3.91	3.41
	$S_{\Sigma} = 30\%$ $S_a \text{ BB} = 500\%$	3.44	3.03	3.92	3.97	3.96	3.74
0.5° × 0.667°	$S_{\Sigma} = 30\%$ $S_a \text{ BB} = 500\%$	3.57	3.14	3.93	3.98	3.97	3.82

Title Page

Abstract

Introduction

Conclusions

References

Tables

Figures

◀

▶

◀

▶

Back

Close

Full Screen / Esc

Printer-friendly Version

Interactive Discussion

## Top-down estimates of biomass burning emissions of black carbon

Y. H. Mao et al.

Title Page

Abstract

Introduction

Conclusions

References

Tables

Figures

⏪

⏩

◀

▶

Back

Close

Full Screen / Esc

Printer-friendly Version

Interactive Discussion

**Table 2.** Monthly biomass burning BC emissions from three regions in the WUS (see Fig. 1) and anthropogenic BC emissions from the WUS for May–October 2006 (unit: Gg). A priori GFEDv2, the a posteriori biomass burning emissions from inversions at  $2^\circ \times 2.5^\circ$  and at  $0.5^\circ \times 0.667^\circ$  horizontal resolutions are shown. Also shown are GFEDv3 and the Fire Locating and Monitoring of Burning Emissions (FLAMBE) for comparison.

Inventory	Source region	BC Emissions (Gg), 2006						
		May	Jun	Jul	Aug	Sep	Oct	Jul–Sep total
A Priori GFEDv2	RM	0.13	0.19	0.93	1.26	0.82	0.17	3.01
	CSW	0.14	0.49	0.60	0.48	0.99	0.26	2.07
	PNW	0.09	0.02	0.23	0.98	0.46	0.19	1.67
	Total	0.36	0.7	1.76	2.72	2.27	0.62	6.75
	ANTHWUS	6.13	5.98	5.85	5.82	5.92	6.15	17.59
A Posteriori ( $2^\circ \times 2.5^\circ$ )	RM	1.72	1.62	7.83	7.60	5.77	1.55	21.2
	CSW	2.11	1.38	2.63	1.41	4.84	3.44	8.88
	PNW	1.16	0.19	0.55	0.89	0.21	0.70	1.65
	Total	4.99	3.19	11.01	9.9	10.82	5.69	31.73
	ANTHWUS	3.39	3.26	2.79	2.81	3.47	3.11	9.07
A Posteriori ( $0.5^\circ \times 0.667^\circ$ )	RM	2.23	2.20	5.99	4.08	4.23	1.55	14.3
	CSW	1.95	2.14	0.26	0.08	1.17	1.50	1.51
	PNW	0.87	0.19	0.95	1.90	0.52	0.57	3.37
	Total	5.05	4.53	7.2	6.06	5.92	3.62	19.18
	ANTHWUS	3.30	2.96	3.61	3.07	4.56	3.95	11.24
GFEDv3	RM	0.00	0.12	0.61	1.47	0.73	0.05	2.81
	CSW	0.02	0.30	0.49	0.48	1.31	0.11	2.28
	PNW	0.00	0.01	0.27	1.31	0.56	0.02	2.14
	Total	0.02	0.43	1.37	3.26	2.6	0.18	7.23
FLAMBE	RM	0.47	0.82	4.73	5.96	3.86	0.21	14.55
	CSW	0.61	3.25	5.78	1.96	9.05	0.62	16.79
	PNW	0.26	0.28	2.35	3.97	2.40	0.29	8.72
	Total	1.34	4.35	12.86	11.89	15.31	1.12	40.06

Top-down estimates  
of biomass burning  
emissions of black  
carbon

Y. H. Mao et al.

Title Page

Abstract

Introduction

Conclusions

References

Tables

Figures

◀

▶

◀

▶

Back

Close

Full Screen / Esc

Printer-friendly Version

Interactive Discussion

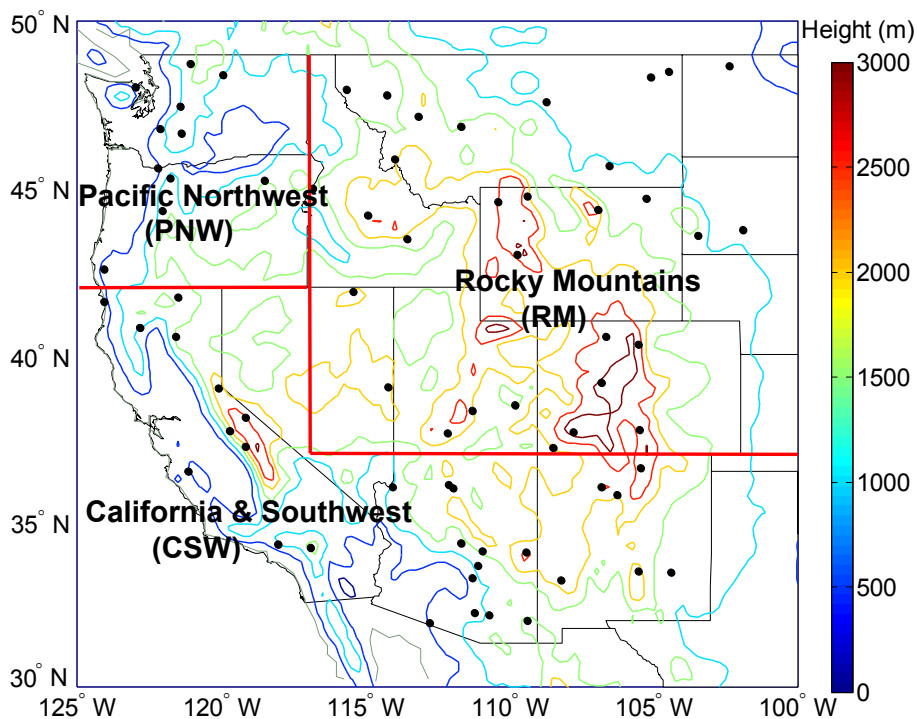


**Fig. 1.** The 69 IMPROVE sites (black dots) used in this study (data available at <http://vista.cira.colostate.edu/improve/>). Also shown are the three biomass burning regions used to define the state vector of the inversion analyses: the Rocky Mountains (RM), California and the Southwest (CSW), and the Pacific Northwest (PNW). Terrain heights are indicated by color contours.

## Top-down estimates of biomass burning emissions of black carbon

Y. H. Mao et al.

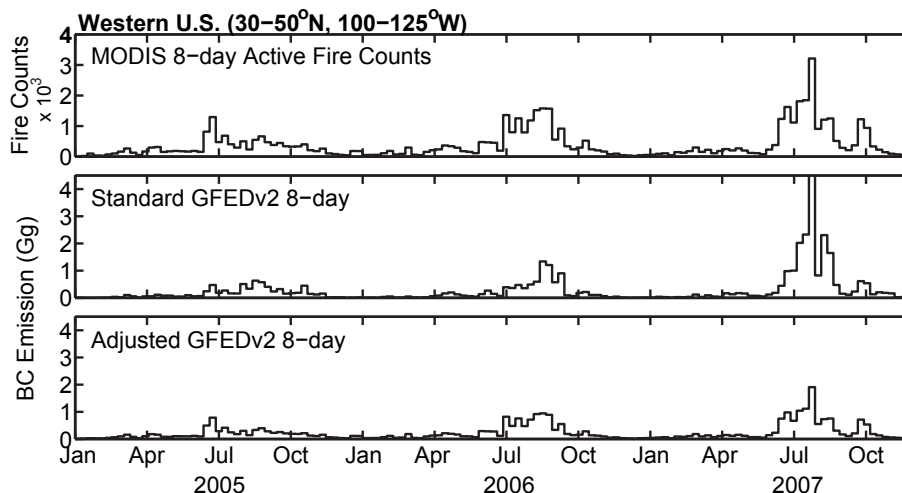


**Fig. 2.** MODIS active fire counts (top panel) and the GFEDv2 biomass burning emissions of BC (middle and bottom panels) summed over the Western US (WUS) from 2005 to 2007. The emissions before (middle panel) and after (bottom panel) applying spatiotemporal adjustments based on the active fire counts (see text for details on the adjustments) are both shown. Data shown here has an 8 day temporal resolution. MODIS active fire counts data are available at <ftp://fuoco.geog.umd.edu>. GFED data are available at [http://daac.ornl.gov/VEGETATION/guides/global\\_fire\\_emissions\\_v2.1.html](http://daac.ornl.gov/VEGETATION/guides/global_fire_emissions_v2.1.html).

Title Page

Abstract

Introduction

Conclusions

References

Tables

Figures

◀

▶

◀

▶

Back

Close

Full Screen / Esc

Printer-friendly Version

Interactive Discussion

## Top-down estimates of biomass burning emissions of black carbon

Y. H. Mao et al.

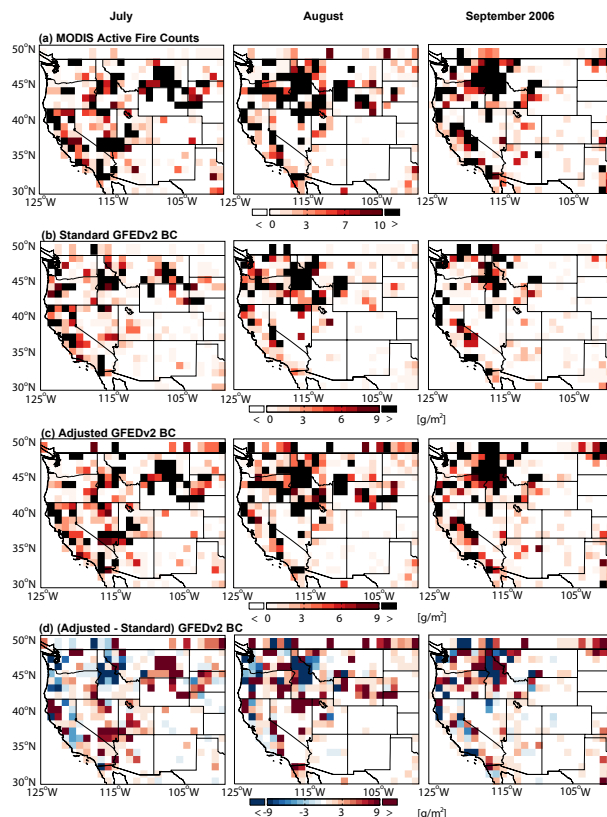


**Fig. 3.** Monthly MODIS active fire counts and biomass burning emissions of BC (unit:  $\text{g m}^{-2}$ ) in the WUS for July, August, and September 2006, respectively: **(a)** MODIS active fire counts, **(b)** standard GFEDv2 BC emissions, **(c)** GFEDv2 BC emissions adjusted spatiotemporally based on the active fire counts (see text for details on the adjustments), and **(d)** the difference between **(c)** and **(b)**.

## Top-down estimates of biomass burning emissions of black carbon

Y. H. Mao et al.

Title Page

Abstract

Introduction

Conclusions

References

Tables

Figures

◀

▶

◀

▶

Back

Close

Full Screen / Esc

Printer-friendly Version

Interactive Discussion

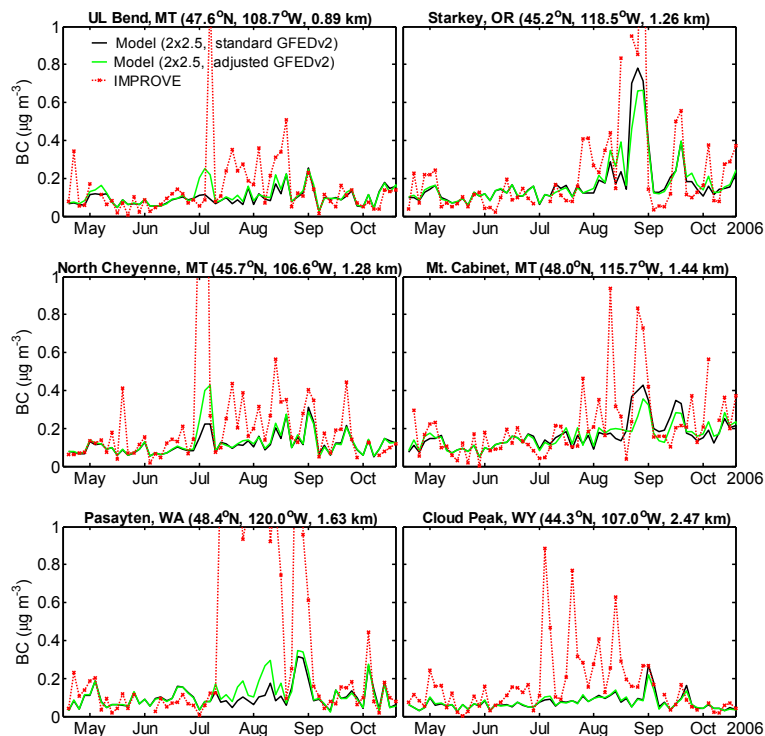


**Fig. 4.** Observed (red line) and simulated daily surface BC concentrations ( $\mu\text{g m}^{-3}$ ) at selective IMPROVE sites for May–October 2006. Values shown are daily averages for every three days. Model results are from simulations at  $2^\circ \times 2.5^\circ$  horizontal resolution and with the standard (black line) and the adjusted (green line; see Figs. 1 and 2) GFEDv2 emissions. Model results are sampled at the time and location of IMPROVE observations.

## Top-down estimates of biomass burning emissions of black carbon

Y. H. Mao et al.

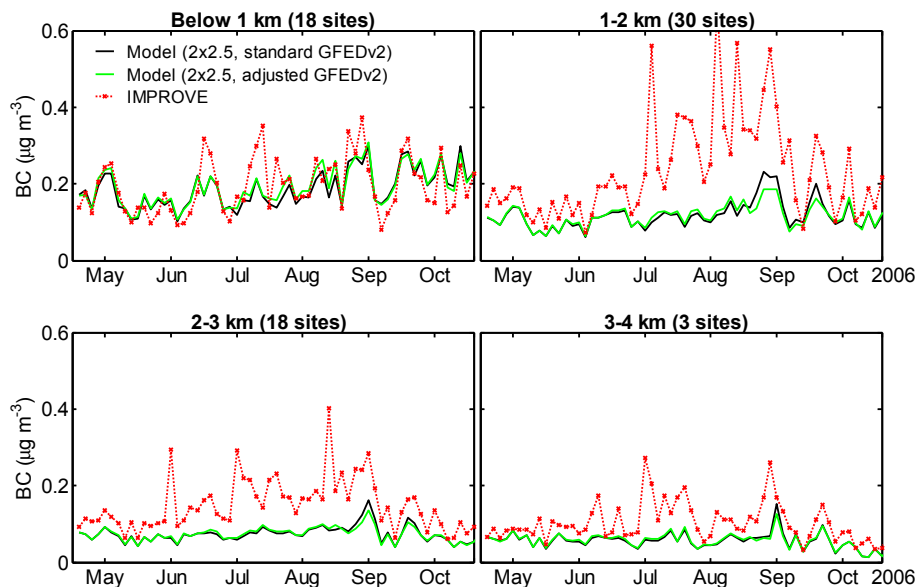


**Fig. 5.** Observed (red line) and simulated daily surface BC concentrations ( $\mu\text{g m}^{-3}$ ) at IMPROVE sites for May–October 2006, averaged for four altitude ranges: below 1 km (averages at 18 sites), 1–2 km (averages at 30 sites), 2–3 km (averages at 18 sites), and above 3 km (averages at 3 sites). Model results are from simulations at  $2^\circ \times 2.5^\circ$  horizontal resolution and with the standard (black line) and the adjusted (green line; see Figs. 1 and 2) GFEDv2 emissions.

## Top-down estimates of biomass burning emissions of black carbon

Y. H. Mao et al.

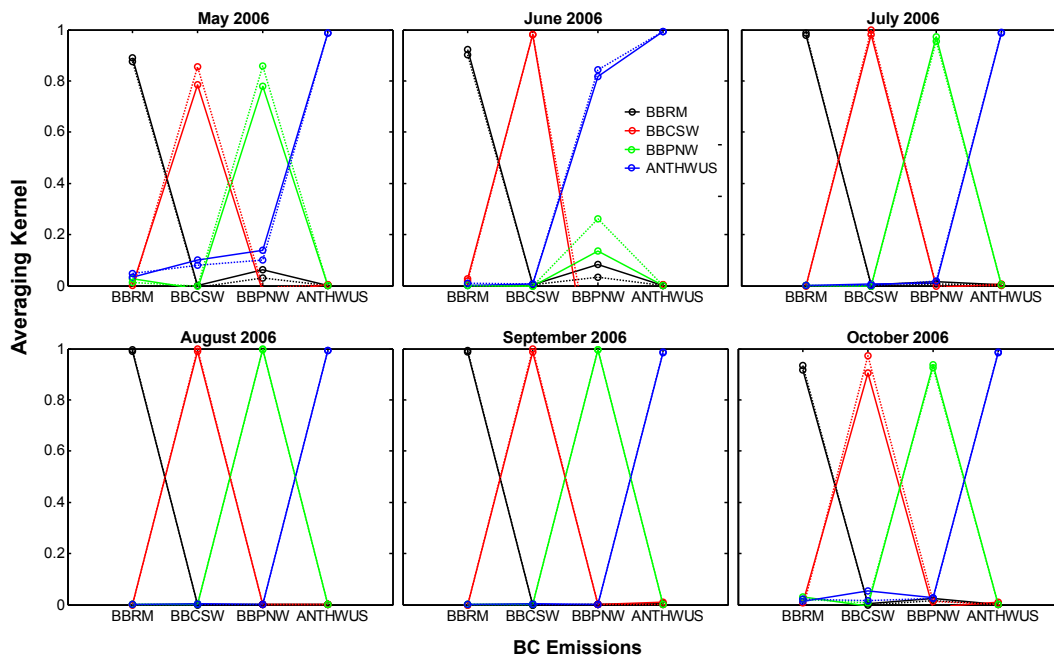


**Fig. 6.** The averaging kernels for inversions (May–October 2006) of BC emissions in the WUS, with each line corresponding to an emission source or source region: biomass burning emissions in the Rockies (BBRM, black line), biomass burning emissions in California and the South-west (BBCSW, red line), biomass burning emissions in the Pacific Northwest (BBPNW, green line), and anthropogenic emissions in the Western US (ANTHWUS, blue line). Results here are from simulations at  $2^\circ \times 2.5^\circ$  (solid line) and at  $0.5^\circ \times 0.667^\circ$  (dotted line) horizontal resolutions and with best set of error characterizations (30 % for observations and 500 % for biomass burning emissions; bottom two rows in Table 1).

[Title Page](#)
[Abstract](#)
[Introduction](#)
[Conclusions](#)
[References](#)
[Tables](#)
[Figures](#)
[Back](#)
[Close](#)
[Full Screen / Esc](#)
[Printer-friendly Version](#)
[Interactive Discussion](#)

## Top-down estimates of biomass burning emissions of black carbon

Y. H. Mao et al.

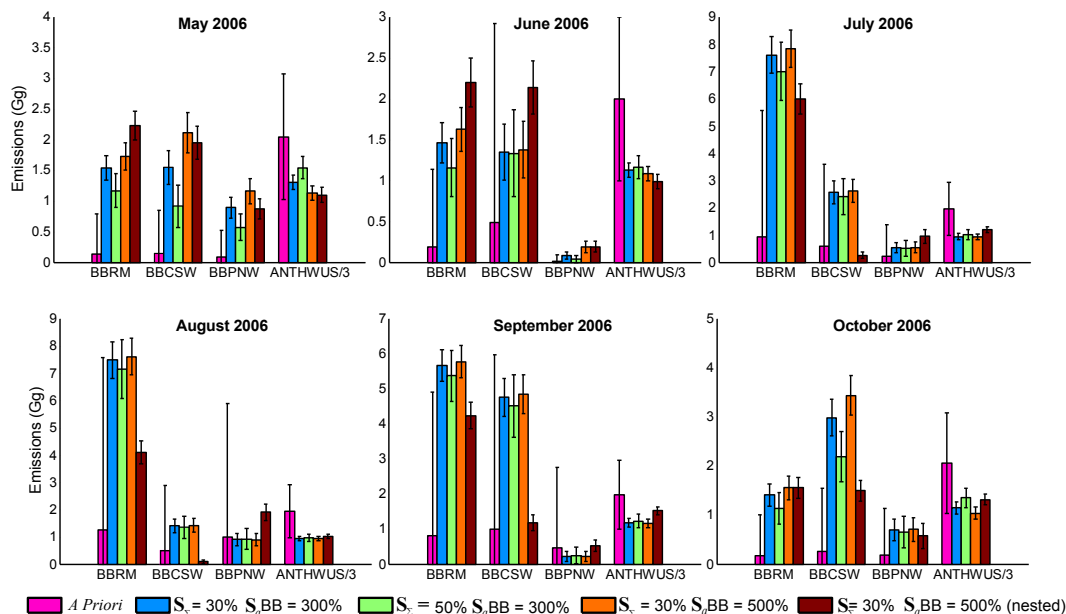


**Fig. 7.** Monthly BC emissions in the WUS for May–October 2006: a priori BC emissions (pink); a posteriori emissions of biomass burning BC from the Rockies (BBRM), from California and the Southwest (BBCSW), and from the Pacific Northwest (BBPNW), and a posteriori emissions of anthropogenic BC from the WUS (ANTHWUS). A posteriori emissions from inversions at  $2^\circ \times 2.5^\circ$  (blue, green, orange) and at  $0.5^\circ \times 0.667^\circ$  (red) horizontal resolutions, color-coded by error characterizations (see text for details), are shown. For the purpose of clarity, anthropogenic emissions are divided by three in the figures. Error bars represent estimated uncertainties of the emissions.

## Top-down estimates of biomass burning emissions of black carbon

Y. H. Mao et al.

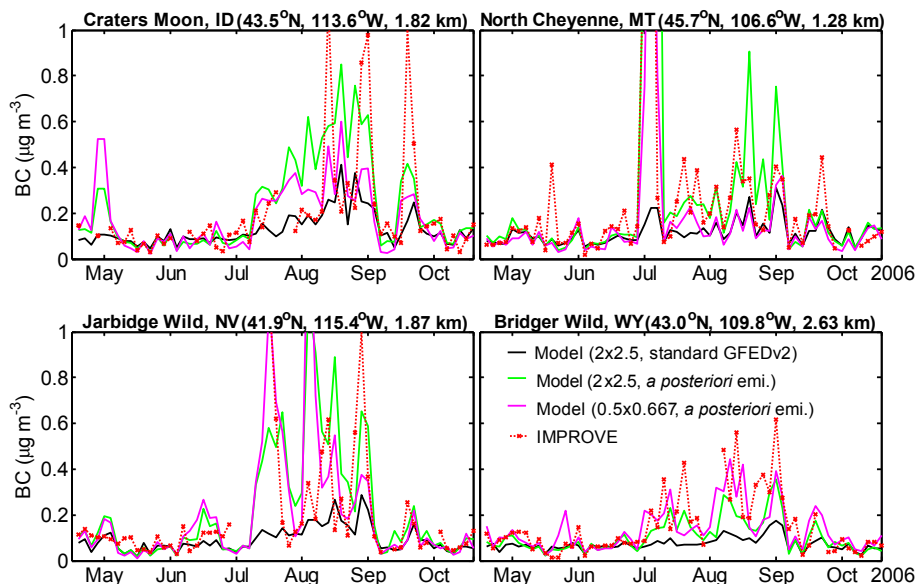


**Fig. 8.** Observed (red line) and simulated daily surface BC concentrations ( $\mu\text{g m}^{-3}$ ) at four IMPROVE sites in the Rockies for May–October 2006. Values shown are daily averages for every three days. Shown are results from simulations with the standard GFEDv2 emissions (black line,  $2^\circ \times 2.5^\circ$ ) and with the a posteriori emissions (green line,  $2^\circ \times 2.5^\circ$ ; pink line,  $0.5^\circ \times 0.667^\circ$ ).

[Title Page](#)
[Abstract](#)
[Introduction](#)
[Conclusions](#)
[References](#)
[Tables](#)
[Figures](#)
[Back](#)
[Close](#)
[Full Screen / Esc](#)
[Printer-friendly Version](#)
[Interactive Discussion](#)

## Top-down estimates of biomass burning emissions of black carbon

Y. H. Mao et al.

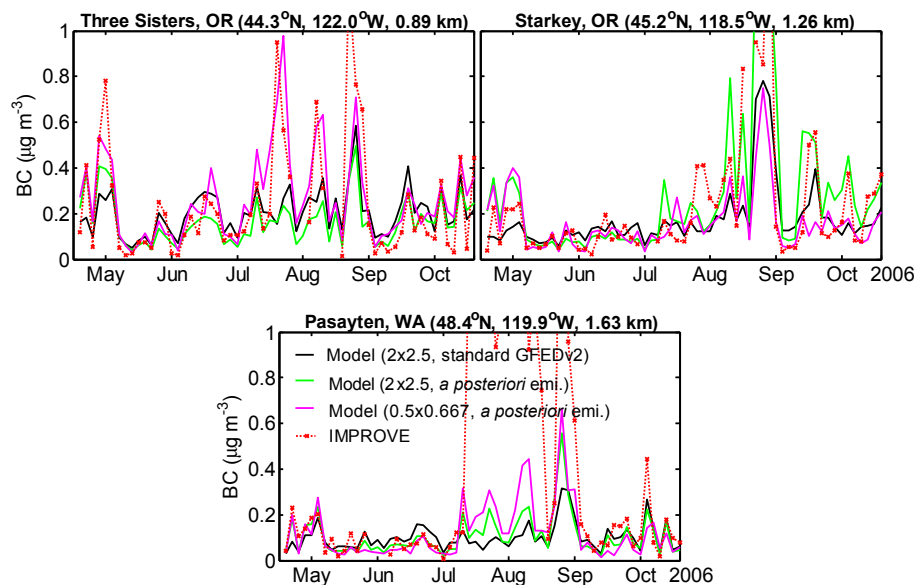


Fig. 9. Same as Fig. 8, but for three IMPROVE sites in the Pacific Northwest.

[Title Page](#)[Abstract](#)[Introduction](#)[Conclusions](#)[References](#)[Tables](#)[Figures](#)[◀](#)[▶](#)[◀](#)[▶](#)[Back](#)[Close](#)[Full Screen / Esc](#)[Printer-friendly Version](#)[Interactive Discussion](#)



## Top-down estimates of biomass burning emissions of black carbon

Y. H. Mao et al.

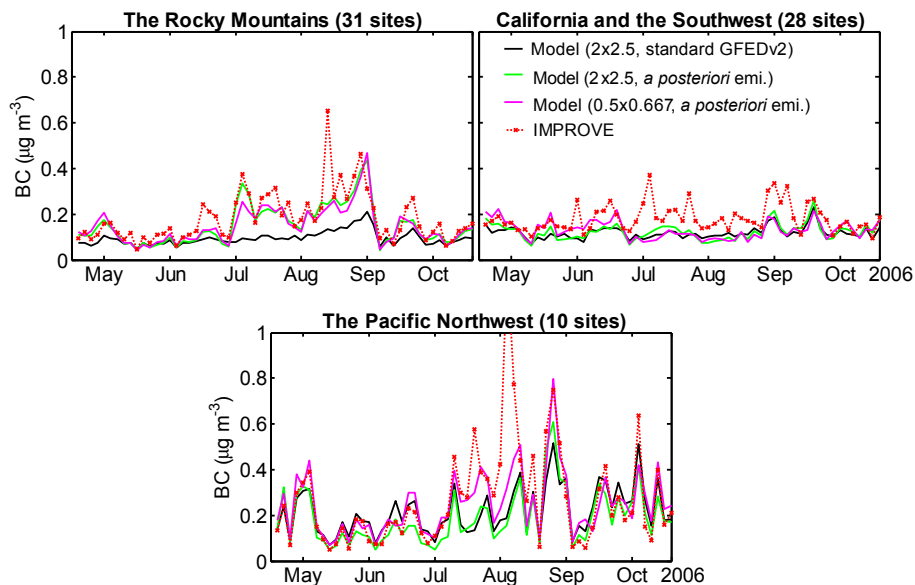


**Fig. 11.** Observed (red line) and simulated daily surface BC concentrations ( $\mu\text{g m}^{-3}$ ) averaged at IMPROVE sites in the Rockies (top left panel, 31 sites), in California and the Southwest (top right panel, 28 sites), and in the Pacific Northwest (bottom panel, 10 sites) for May–October 2006. Shown are results from simulations with the standard GFEDv2 emissions (black line,  $2^\circ \times 2.5^\circ$ ) and with the a posteriori emissions (green line,  $2^\circ \times 2.5^\circ$ ; pink line,  $0.5^\circ \times 0.667^\circ$ ).

## Top-down estimates of biomass burning emissions of black carbon

Y. H. Mao et al.

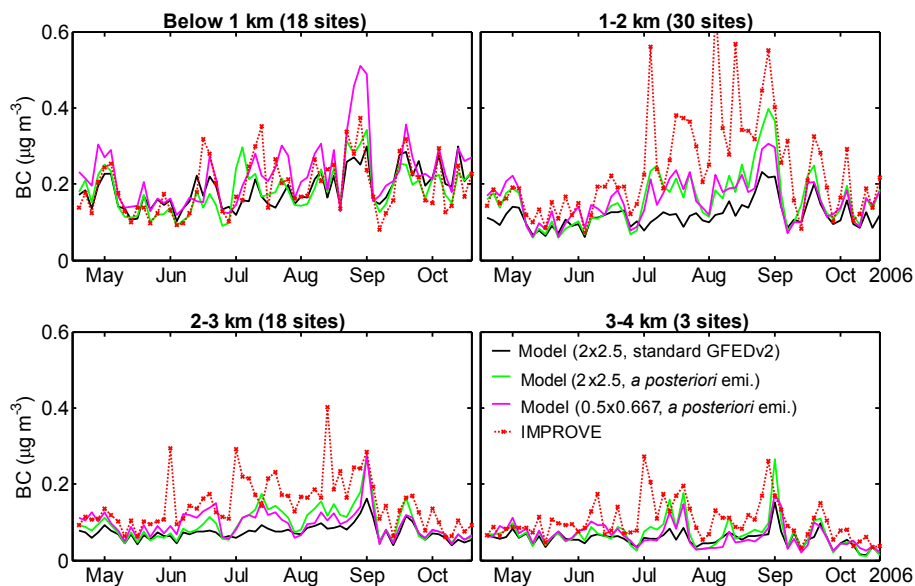


**Fig. 12.** Same as Fig. 5, but for simulations with the standard GFEDv2 emissions (black line,  $2^\circ \times 2.5^\circ$ ) and with the a posteriori emissions (green line,  $2^\circ \times 2.5^\circ$ ; pink line,  $0.5^\circ \times 0.667^\circ$ ).

Title Page

Abstract

Introduction

Conclusions

References

Tables

Figures

◀

▶

◀

▶

Back

Close

Full Screen / Esc

Printer-friendly Version

Interactive Discussion

## Top-down estimates of biomass burning emissions of black carbon

Y. H. Mao et al.

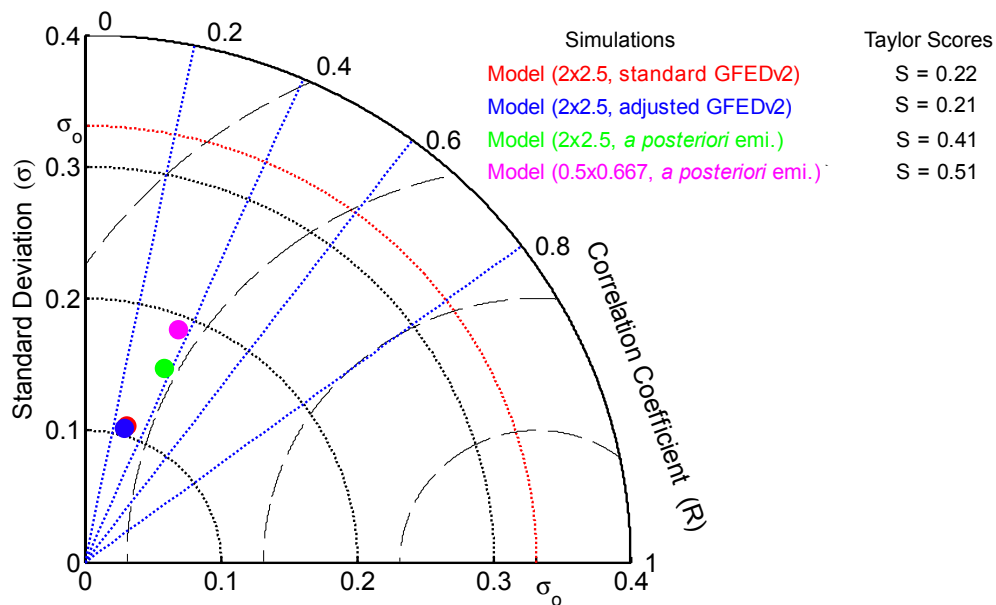


**Fig. 13.** Taylor diagram and Taylor scores for simulations with the standard GFEDv2 emissions (red dot,  $2^\circ \times 2.5^\circ$ ), with the adjusted GFEDv2 emissions (blue dot,  $2^\circ \times 2.5^\circ$ ), and with the a posteriori emissions (green dot,  $2^\circ \times 2.5^\circ$ ; pink dot,  $0.5^\circ \times 0.667^\circ$ ) for May–October 2006. Values are averages for the 69 IMPROVE sites in the WUS (Fig. 1).

Title Page

Abstract Introduction

Conclusions References

Tables Figures

⏪ ⏩

⏴ ⏵

Back Close

Full Screen / Esc

Printer-friendly Version

Interactive Discussion

## Top-down estimates of biomass burning emissions of black carbon

Y. H. Mao et al.

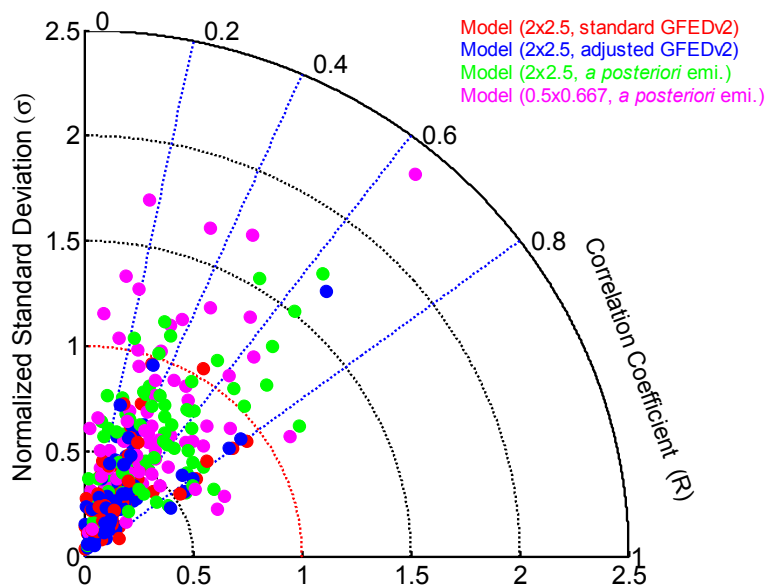


**Fig. 14.** Same as Fig. 13, but for the 69 individual IMPROVE sites in the WUS (Fig. 1). The standard deviation for each site is normalized by the standard deviation of the observations at that site.

[Title Page](#)
[Abstract](#)
[Introduction](#)
[Conclusions](#)
[References](#)
[Tables](#)
[Figures](#)
[Back](#)
[Close](#)
[Full Screen / Esc](#)
[Printer-friendly Version](#)
[Interactive Discussion](#)